



CHORUS

This is the accepted manuscript made available via CHORUS. The article has been published as:

Thermorefractive noise of finite-sized cylindrical test masses

D. Heinert, A. G. Gurkovsky, R. Nawrodt, S. P. Vyatchanin, and K. Yamamoto

Phys. Rev. D **84**, 062001 — Published 2 September 2011

DOI: [10.1103/PhysRevD.84.062001](https://doi.org/10.1103/PhysRevD.84.062001)

Thermorefractive noise of finite-sized cylindrical test masses

D. Heinert,¹ A. G. Gurkovsky,² R. Nawrodt,¹ S. P. Vyatchanin,^{2,*} and K. Yamamoto^{3,†}

¹*Institut für Festkörperphysik, Friedrich-Schiller-Universität Jena, D-07743 Jena, Germany*

²*Faculty of Physics, Moscow State University, Moscow, 119991 Russia*

³*Istituto Nazionale di Fisica Nucleare, Sezione di Padova, Via Marzolo 8, 35131 Padova, Italy*

We present an analytical solution for the effect of thermorefractive noise considering finite-sized cylindrical test masses. For crystalline materials at low temperatures the effect of finite dimensions becomes important. The calculations are independently performed using the Fluctuation-Dissipation-Theorem and Langevin's approach. Our results are applied to the input test mass of the current and future cryogenic gravitational wave detectors CLIO, LCGT, and ET and are compared to the respective standard quantum limit. For a substrate temperature of 10 K we find that the thermorefractive noise amplitude of the silicon input test mass in ET is only a factor of 2 below the standard quantum limit for frequencies above 500 Hz. Thus, thermorefractive noise of the input test mass could become a severe limitation if one uses techniques to beat the standard quantum limit like, e.g., squeezing. In contrast the effect of thermorefractive noise of the input test mass is negligible for CLIO and LCGT.

PACS numbers: 04.80.Cc, 04.30.Db, 04.80.Nn

I. INTRODUCTION

Thermal noise basing on the change of the refractive index on temperature - thermorefractive (TR) noise - is one key noise process in the design of interferometric gravitational wave detectors [1–3]. Wherever the laser beam passes matter, the temperature fluctuations within the substrate will cause a change of the refractive index and, consequently, will change the phase of the traveling beam. In the case of a Michelson interferometer with Fabry-Perot cavities in its arms the beam splitter and the input test mass (ITM) of the arm resonators represent two components that are probed by the light and, thus, introduce TR noise to the interferometer's output. TR noise is increasingly important in optical high-Q microresonators [4, 5] as it was measured in optical fibers [6], in optical microspheres [7], and in microtoroids [8]. It can also play a role in the frequency stabilization of lasers [9], where the beam passes the cavity mirror substrates.

Braginsky et al. were the first to realize the influence of TR noise on the field of gravitational wave detection [10]. They investigated the effect of TR noise of the multilayer coating stacks attached onto the optical components. In 2004 Braginsky and Vyatchanin presented an analytical solution for the TR noise of an infinite disc with finite thickness [11]. While these first publications in the field used the Langevin approach, Levin introduced a new direct approach of noise calculation [12] utilizing the Fluctuation-Dissipation-Theorem and applied it on TR noise in 2008 [13]. In that work he validated the result of the model of the infinite disc. With the same model of the infinite disc the TR noise level of the GEO600 beam

splitter was determined in 2009 [14]. There the effect of a standing wave emerging in the substrate was considered.

Recent TR noise investigations [15, 16] were related to the Einstein telescope (ET) as a planned third generation gravitational wave detector. For the ET low frequency detector the ITM and ETM (end test mass) are proposed to be made from crystalline silicon instead of fused silica and should be operated at cryogenic temperatures. The change of the material and the temperature regime drastically alters the thermal parameters of the substrate, on which a TR noise calculation bases. Thus, it is important to extend the current model to consider the finite radial dimension of the substrate. Our analysis reveals that the effect of the finite size is to be taken into account for cooled and crystalline substrates. Next to ET also CLIO and LCGT [2] exhibit crystalline substrates at low temperatures and are under investigation in this work.

In this paper we present an analytical solution of TR noise for a finite-sized cylinder. The results are derived independently by the Langevin approach as well as Levin's approach. Section II refers to the simplified case of a readout that is homogeneous along the cylindrical axis, while section III takes the effect of standing waves into account. The analytical results are finally applied to several interferometer geometries and confirmed by a finite element analysis in section IV. For this purpose we focus on silicon and sapphire as promising cryogenic substrate materials.

II. SIMPLE MODEL

This section shows the derivation of TR noise of a finite-sized cylinder for the case of a pure travelling wave. In this simple model we neglect the interferometric effect of standing waves. To perform this calculation we use the coordinate system shown in Fig. 1. For the problem

* svyatchanin@physics.msu.ru

† Present address: Institute for Cosmic Ray Research, The University of Tokyo, 5-1-5 Kashiwa-no-Ha, Kashiwa, Chiba 277-8582, Japan

is completely radial symmetric we choose cylinder coordinates (r, φ, z) to obtain an easy formulation of the problem.

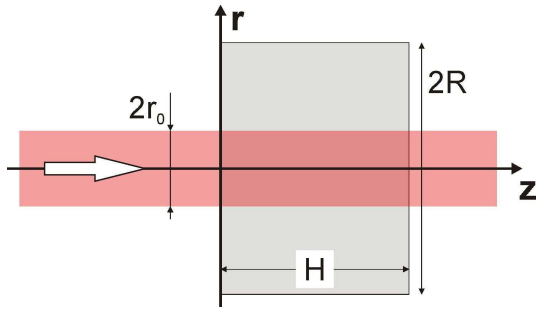


FIG. 1. Problem geometry with the substrate (height H , diameter $2R$), the laser beam (diameter $2r_0$), and the radial coordinate system (r, z) .

Let us remember the main process again. Light is approaching from the left, then travels through the substrate, where it probes the refractive index N of the medium and is transmitted to the right.

The transmitted beam experiences an optical path difference z due to the temperature field $T(\vec{r})$ in the substrate. At a homogeneous temperature T_0 this path is assumed to have the length z_0 . For small temperature fluctuations the path change can be calculated in a first order approximation with the intensity profile of the laser beam

$$z - z_0 = \frac{1}{\pi r_0^2} \int \beta(T_0)(T(\vec{r}) - T_0) e^{-\frac{r^2}{r_0^2}} dV \quad (1)$$

$$= \int t(\vec{r})(T(\vec{r}) - T_0) dV. \quad (2)$$

Here $\beta = dN/dT$ represents the thermo-optical parameter and r_0 is the laser beam radius where intensity drops to $1/e$. The factor in front of the integral arises from the fact, that a constant thermal field $T(\vec{r}) = T$ leads to $z - z_0 = \beta H(T - T_0)$, where H is the height of the cylinder. Using this definition of z the resulting TR noise spectrum $S_z(\omega)$ is expressed as an equivalent mirror displacement. Such a choice allows an easy comparison of the TR noise level with other noise sources.

A. Levin's approach

The typical way to calculate TR noise via the Fluctuation-Dissipation-Theorem by Levin [13] consists of three steps. At first one has to apply a virtual source of entropy. Using this source term the heat equation is solved in a second step to obtain the temperature distribution within the substrate. Then the temperature field allows to calculate the rate of energy dissipation W_{diss} . Finally, the power spectral density $S_z(\omega)$ for fluctuations

of the optical path length z at the frequency ω follows from

$$S_z(\omega) = \frac{8k_B T_0}{\omega^2} \frac{W_{\text{diss}}}{F_0^2}. \quad (3)$$

In this equation k_B is Boltzmann's constant, T_0 is the ambient temperature, and F_0 is a normalization constant ensuring that the noise spectrum does not depend on the amplitude of the virtually applied entropy. As Levin's approach is a direct formulation of the fluctuation-dissipation theorem by Callen and Welton it is valid for any linear system at arbitrary frequencies [17]. Only the calculation of the dissipated power may vary with respect to different frequency regimes. This point is further discussed in Sec. IV B.

Following Levin's approach we start with the application of an imaginary heat density q with the profile $t(\vec{r})$ given by Eq. (2). This heat term reads

$$q(\vec{r}, t) = T(\vec{r}, t) F_0 \cos(\omega t) t(\vec{r}) \quad (4)$$

$$= T(\vec{r}, t) F_0 \cos(\omega t) \frac{\beta}{\pi r_0^2} e^{-\frac{r^2}{r_0^2}}, \quad (5)$$

with temperature T and the scaling constant F_0 . Here the cylinder is oriented in a way that its axis of radial symmetry coincides with the z -axis. Eq. (5) can be further simplified by considering only small temperature fluctuations. In this case we can treat $T(\vec{r}, t)$ as nearly constant and replace it by the constant ambient temperature T_0 with a negligible error. In the approximation of the simple model the inserted heat is independent from z and reads

$$q(\vec{r}, t) = \Re \left(\frac{\beta}{\pi r_0^2} T_0 F_0 e^{-\frac{r^2}{r_0^2}} e^{i\omega t} \right) = \Re [q(r) e^{i\omega t}], \quad (6)$$

where \Re represents the real part. The last equality of Eq. (6) defines the spatial heat density $q(r)$.

To obtain an expression for the dissipated power we have to derive a solution of the heat equation $T(\vec{r}, t)$ in our second step. For a material exhibiting an isotropic thermal conductivity κ the heat equation reads

$$C_p \dot{T}(\vec{r}, t) - \kappa \Delta T(\vec{r}, t) = \dot{q}(\vec{r}, t), \quad (7)$$

where C_p is the specific heat per unit volume and q is the introduced heat density given by Eq. (6). The cylinder is assumed to satisfy adiabatic conditions at the boundary, i.e., vanishing heat flow through the boundary. A justification of this assumption is given in App. A. Using cylindrical coordinates (r, φ, z) we obtain

$$\left. \frac{\partial T}{\partial z} \right|_{z=0, H} = \left. \frac{\partial T}{\partial r} \right|_{r=R} = 0. \quad (8)$$

The heat equation is easily solved by means of a Fourier transform. But we have to account for the boundary condition by the choice of an adapted set of basis functions. The new basis is illustrated for the temperature field as

$$T(r, z) = \sum_{n=0}^{\infty} \sum_{m=0}^{\infty} T_{nm} J_0(k_n r) \cos(l_m z), \quad (9)$$

where J_0 represents the Bessel function of the first kind. The boundary conditions constrain the parameters k_n and l_m to the following discrete values

$$k_n = \frac{a_n}{R}, \text{ with } J_1(a_n) = 0, \quad (10)$$

$$l_m = m \frac{\pi}{H}. \quad (11)$$

With the help of the heat equation [Eq. (7)] we can express the coefficients T_{nm} by the coefficients of the inserted heat q_{nm}

$$\begin{aligned} i\omega C_p T_{nm} + \kappa (k_n^2 + l_m^2) T_{nm} &= i\omega q_{nm} \\ \Rightarrow T_{nm} &= \frac{q_{nm}}{C_p - i\frac{\kappa}{\omega} (k_n^2 + l_m^2)}. \end{aligned} \quad (12)$$

Within the simple model discussed in this section the inserted heat is independent from z . This leads to a cancellation of all terms q_{nm} with $m \neq 0$. Consequently, also the temperature distribution will be independent from the z -coordinate and we can omit the index m for the remaining part of this subsection. To derive the coefficients q_n we make use of the following orthogonality relation for Bessel functions [18, Eq. 11.4.5]

$$\int_0^1 J_0(a_n \rho) J_0(a_m \rho) \rho d\rho = \frac{1}{2} [J_0(a_n)]^2 \delta_{nm}, \quad (13)$$

leading to the following expression for the coefficient q_n

$$q_n = \frac{1}{R^2} \frac{2}{[J_0(a_n)]^2} \int_0^R q(r) J_0(k_n r) r dr. \quad (14)$$

In the last step of Levin's scheme we have to determine the amount of dissipated power W_{diss} within the cylinder. As every heat flow is irreversible it consumes mechanical energy and transforms it into thermal energy. Therefore the dissipated energy should be linked to the amount of heat flowing within the cylinder. A rigorous treatment of this problem [19] yields

$$W_{\text{diss}} = \frac{1}{2T_0} \int_V \kappa (\nabla T)^2 dV. \quad (15)$$

Due to the radial symmetry of our problem Eq. (15) simplifies to

$$W_{\text{diss}} = \frac{\pi H \kappa}{T_0} \int_0^R \left| \frac{\partial}{\partial r} T \right|^2 r dr. \quad (16)$$

After inserting the basis decomposition of $T(r)$ the following orthogonality condition for Bessel functions [18, Eq. 11.4.5]

$$\int_0^1 J_1(a_m \rho) J_1(a_n \rho) \rho d\rho = \frac{1}{2} [J_1'(a_n)]^2 \delta_{mn}, \quad (17)$$

leads to

$$\int_0^R \left| \frac{\partial}{\partial r} T \right|^2 r dr = \frac{1}{2} \sum_{n=0}^{\infty} |T_n|^2 a_n^2 [J_1'(a_n)]^2. \quad (18)$$

Using the relations $[J_1'(a_n)]^2 = [J_0(a_n)]^2$ and $a_0 = 0$ and combining Eqs. (3), (12), (14), (16), and (18) we finally arrive at an expression for the displacement noise for a read out homogeneous along the z -direction.

$$\begin{aligned} S_z^{(\text{hom})}(\omega) &= \frac{16}{\pi} k_B T_0^2 \frac{H R^2}{r_0^4} \frac{\kappa \beta^2}{C_p^2} \\ &\times \sum_{n=1}^{\infty} \frac{k_n^2}{[J_0(a_n)]^2} \frac{K_n^2}{\omega^2 + \frac{\kappa^2}{C_p^2} k_n^4}, \end{aligned} \quad (19)$$

with

$$K_n = \int_0^1 J_0(a_n \rho) e^{-\left(\frac{R}{r_0} \rho\right)^2} \rho d\rho. \quad (20)$$

Note that this result is only valid if the substrate is probed by a single transmission of the laser beam. In a gravitational wave detector the laser beam passes the ITM substrate, reaches the coating for the arm cavity at the end of the ITM, interacts with the cavity, and finally passes the ITM substrate a second time on its way out of the arm. Taking this second probe of the substrate into account we have to multiply the power spectrum of thermal noise $S_z(\omega)$ by the factor of 4. On the other hand we can interpret $S_z(\omega)$ in Eq. (19) as the noise spectrum of an equivalent mirror displacement.

B. Langevin approach

In 1908 Langevin investigated the Brownian motion of a particle suspended in a fluid [20]. For this purpose he modeled the statistical impacts of the fluid molecules on the particle by a fluctuating force term in the equation of motion.

We fully adopt his approach to the case of temperature fluctuations as described in Refs. [10, 21]. Therefore, we have to consider the heat equation with a generalized fluctuating force term $F(\vec{r}, t)$

$$\dot{T}(\vec{r}, t) - a^2 \Delta T(\vec{r}, t) = F(\vec{r}, t). \quad (21)$$

The coefficient a^2 represents the temperature conductivity and is given by $a^2 = \kappa/C_p$, Δ is the Laplace operator. In analogy to Langevin the fluctuating force term is assumed to be uncorrelated in time, i.e., the time scale for a change of temperature is long compared to changes of $F(\vec{r}, t)$. Mathematically this behavior is expressed as

$$\langle F(\vec{r}, t) F(\vec{r}', t') \rangle = C(\vec{r}, \vec{r}') \delta(t - t'), \quad (22)$$

where the brackets represent the thermodynamic ensemble average. Braginsky et al. [10] calculated the space correlator C yielding

$$C(\vec{r}, \vec{r}') = -2k_B T_0^2 \frac{\kappa}{C_p^2} \Delta \delta(\vec{r} - \vec{r}'), \quad (23)$$

where the Laplace operator Δ is acting on the δ -distribution. The same result was obtained earlier in Ref. [21].

At this point we introduce a temperature \bar{T} that is averaged with the spatial profile of the laser beam intensity as

$$\begin{aligned} \bar{T}(t) &= \frac{1}{\pi r_0^2 H} \int_V T(\vec{r}, t) e^{-\frac{r^2}{r_0^2}} dV \\ &= T_0 + \frac{1}{\beta H} (z - z_0). \end{aligned} \quad (24)$$

The last equality reveals a close connection of this averaged temperature and Eq. (2). The results of the calculations using Langevin approach coincide with Eq. (19) as the result from Levin's method. Some mathematical details are presented in App. B.

III. ADVANCED MODEL

In contrast to the case of a single transmission, the beam splitter and the input test mass of an interferometric gravitational wave detector are probed twice, once by the incoming light and once by the reflected light. As the interferometer is locked both waves show a fixed phase relation leading to the well known phenomenon of standing waves. Thus, nodes of the electric field emerge within the substrate, which are insensitive to changes of the refractive index. On the other hand the TR effect at the antinodes is amplified. In 2009 Benthem and Levin [14] were the first to bring this idea into the field of gravitational wave detection. As they did only show a few calculation steps we give a detailed derivation of the effect of standing waves on TR noise in this section.

A rigorous calculation of the correct averaging is given in App. D. For our noise variable of an effective mirror displacement $z - z_0$ it reveals the following expression

$$\begin{aligned} 2(z - z_0) &= \frac{1}{\pi r_0^2} \int_V \beta(T(\vec{r}) - T_0) \\ &\quad \times 4 \sin^2 \left(\frac{2\pi N}{\lambda_0} z + \varphi_0 \right) e^{-\frac{r^2}{r_0^2}} dV, \end{aligned} \quad (25)$$

where N describes the substrate's refractive index and λ_0 is the vacuum laser wavelength. In the present situation of an arm cavity in resonance the additional phase shift φ_0 reveals to be zero. If we average the effect along the z -coordinate, the \sin^2 -term should be replaced by the factor $1/2$ and we recover the imaginary heat distribution for the homogeneous case. This approximation is justified if the thermal path length is large compared to the periodicity along the z -direction which is roughly given by the laser wavelength. A detailed discussion about different thermal regimes can be found in section IV. Eq. (25) leads to a new z -dependence for the introduced heat

$$q(r, z) = 2 \frac{\beta}{\pi r_0^2} T_0 F_0 \sin^2 \left(\frac{2\pi N}{\lambda} z \right) e^{-\frac{r^2}{r_0^2}}. \quad (26)$$

A. Levin's approach

To reveal TR noise including the effect of standing waves via the Fluctuation-Dissipation-Theorem we can adopt the formalism of the simple model up to Eq. (12). In the further analysis we cannot neglect the z -dependence and thus now obtain also factors $q_{nm} \neq 0$ for $m \neq 0$. The analytical expression for q_{nm} is derived from the cosine orthogonality relation

$$\int_0^H \cos(l_m z) \cos(l_n z) dz = \frac{1 + \delta_{m0}}{2} H \delta_{mn}, \quad (27)$$

and Eq. (13) to read

$$\begin{aligned} q_{nm} &= \frac{1}{HR^2} \frac{2}{[J_0(a_n)]^2} \frac{2}{1 + \delta_{m0}} \\ &\quad \times \int_0^H \int_0^R q(r, z) J_0(k_n r) r dr \cos(l_m z) dz. \end{aligned} \quad (28)$$

This result allows the calculation of the dissipated power as

$$W_{\text{diss}} = \frac{\pi \kappa}{T_0} \int_V \left(\left| \frac{\partial}{\partial r} T \right|^2 + \left| \frac{\partial}{\partial z} T \right|^2 \right) r dr dz, \quad (29)$$

for the advanced model. One last orthogonality relation shows

$$\int_0^H \sin(l_m z) \sin(l_n z) dz = \frac{1 - \delta_{m0}}{2} H \delta_{mn}. \quad (30)$$

Together with Eqs. (13), (17), and (27) this allows the evaluation of the noise spectrum following the same steps as for the simple model. Taking the effect of standing waves into account we obtain our final expression

$$\begin{aligned} S_z^{(\text{SW})}(\omega) &= \frac{16}{\pi} k_B T_0^2 \frac{\kappa \beta^2}{C_p^2} \frac{HR^2}{r_0^4} \\ &\quad \times \sum_{n=0}^{\infty} \sum_{m=0}^{\infty} \frac{2}{(1 + \delta_{m0})^2} \frac{1}{[J_0(a_n)]^2} K_n^2 L_m^2 \\ &\quad \times \frac{(1 + \delta_{m0}) k_n^2 + (1 - \delta_{m0}) l_m^2}{\omega^2 + \frac{\kappa^2}{C_p^2} (k_n^2 + l_m^2)^2}, \end{aligned} \quad (31)$$

with

$$K_n = \int_0^1 J_0(a_n \rho) e^{-\left(\frac{R}{r_0} \rho\right)^2} \rho d\rho, \quad (32)$$

$$L_m = \int_0^1 \cos(m\pi\zeta) 2 \sin^2 \left(\frac{2\pi N}{\lambda_0} \zeta H \right) d\zeta. \quad (33)$$

As a first cross check we can replace the term $2 \sin^2(x)$ by its average value of 1. Then all coefficients L_m vanish except for $L_0 = 1$. A short calculation respecting $l_0 = 0$ reveals the coincidence of Eq. (31) with the result of the simple model, i.e., Eq. (19).

B. Langevin approach

The new readout variable is connected to an averaged temperature considering the \sin^2 -term for the averaging along the z -coordinate.

$$\bar{T}(t) = \frac{1}{\pi r_0^2 H} \int_V T(\vec{r}, t) 2 \sin^2 \left(\frac{2\pi N}{\lambda_0} z \right) e^{-\frac{r^2}{r_0^2}} dV. \quad (34)$$

Via the autocorrelation function for \bar{T} we obtain the spectral noise density $S_{\bar{T}}(\omega)$ and arrive at the result for $S_z(\omega)$ coinciding with Eq. (31) — for details of the calculations see App. B.

IV. RESULTS

In this section we apply our TR noise expression on current (CLIO) and future (LCGT, ET) gravitational wave detector designs. In the case of ET we only consider the low frequency detector [22]. These three detectors are working in the cryogenic temperature range, where thermal properties significantly differ from everyday experiences. Mainly, the thermal conductivity κ is increased and the specific heat C_p is decreased at temperatures around 20 K compared to their room temperature values. This implicates an increase of the thermal path length $r_{\text{th}} = \sqrt{\kappa/(\omega C_p)}$ at cryogenic temperatures. If the thermal path length reaches the order of the substrate's radial dimension ($r_{\text{th}} \approx R$) we will see an effect of the finite radial dimension.

A. Material properties

Each thermal noise analysis of an interferometer requires knowledge of the thermal properties of the substrate materials. Sapphire is used in CLIO and LCGT while silicon is the likely choice for ET substrates because of its availability in large dimensions. Although the ITM and ETM are operated at low temperatures the beam splitters of CLIO, LCGT, and ET are made from fused silica and operated at room temperature. The necessary thermal properties for a TR noise estimate of these materials are given in Table I.

Due to the large dimensions of the sample it is likely that the thermal conductivity is not limited by surface scattering of phonons. Consequently, we used the bulk values for the coefficient of thermal conductivity in our TR noise estimates. While the parameters of specific heat and thermal conductivity are well known, the thermo-optic parameter introduces a high uncertainty. For silicon β was only measured at temperatures down to 30 K [25]. The assumed values for lower temperatures represent a conservative extrapolation. Tomaru et al. [26] measured β for sapphire at temperatures down to 5 K. But in the temperature range from 5 K to 40 K they were

TABLE I. Assumed thermal properties for silicon and sapphire. The values of the refractive index N and density ρ are assumed to be constant in the temperature region of $T_0 < 30$ K. For fused silica we use the room temperature values for N (neglecting dispersion) and ρ .

Silicon ($N = 3.45$, $\rho = 2331 \text{ kg m}^{-3}$)			
T_0 (K)	C_p/ρ ($\frac{\text{J}}{\text{kgK}}$)	κ ($\frac{\text{W}}{\text{mK}}$)	β ($10^{-6} \frac{1}{\text{K}}$)
10	0.276 [23]	2110 [24]	1.0
20	3.41 [23]	4940 [24]	1.0
30	18.55 [23]	4810 [24]	3.3 [25]
Sapphire ($N = 1.75$, $\rho = 3980 \text{ kg m}^{-3}$)			
T_0 (K)	C_p/ρ ($\frac{\text{J}}{\text{kgK}}$)	κ ($\frac{\text{W}}{\text{mK}}$)	β ($10^{-8} \frac{1}{\text{K}}$)
10	0.091 [24]	2900 [24]	9 [26]
20	0.690 [24]	15700 [24]	9 [26]
30	2.557 [24]	20700 [24]	9 [26]
Fused silica ($N = 1.45$, $\rho = 2202 \text{ kg m}^{-3}$)			
T_0 (K)	C_p/ρ ($\frac{\text{J}}{\text{kgK}}$)	κ ($\frac{\text{W}}{\text{mK}}$)	β ($10^{-6} \frac{1}{\text{K}}$)
290	746 [24]	1.38 [24]	8

only able to present an upper limit due to the accuracy of their experimental setup.

The required geometry and optical parameters for the input test mass and the beam splitter are shown in Table II and Table III, respectively.

TABLE II. Assumed geometrical and optical properties for the input test mass of CLIO, LCGT, and ET. The optical beam radius w_0 (where intensity drops to $1/e^2$) can be calculated from r_0 as $w_0 = \sqrt{2}r_0$.

Parameter	CLIO	LCGT	ET
Material	Sapphire		Silicon
Diameter $2R$ (mm)	100	250	500
Height H (mm)	60	150	460
Wavelength λ_0 (nm)	1064	1064	1550
Beam radius w_0 (mm)	4.89	35	90
Arm cavity finesse	3000	1550	885

B. Numerical results

A qualitative summary of all occurring frequency regimes due to the analytical solution [Eq. (31)] is given in Fig. 2. To obtain some numbers in the spectrum of TR noise we apply our theoretical expression to a silicon test mass at 10 K exhibiting the ET geometry.

Let us begin our discussion at low frequencies (1 Hz) in region I. At this point the thermal path length is larger than the radius of the substrate $r_{\text{th}} > R$. Thus, the virtually inserted heat is able to reach the radial surface of

TABLE III. Assumed geometrical and optical properties for the beam splitter of CLIO, LCGT, and ET. The substrate diameter of the beam splitter does not influence the TR noise level but is given for completeness.

Parameter	CLIO	LCGT	ET
Material	Fused Silica		
Diameter $2R$ (mm)	150	380	500
Height H (mm)	40	120	460
Wavelength λ_0 (nm)	1064	1064	1550
Beam radius w_0 (mm)	4.9	35.4	90

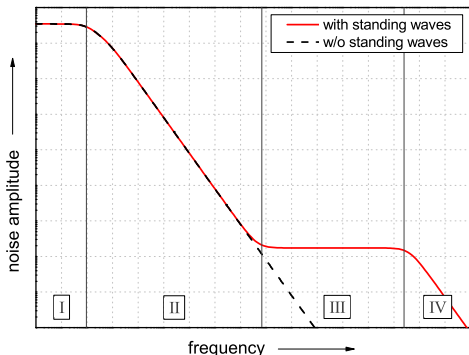


FIG. 2. Schematic TR noise spectrum for a finite-sized cylindrical test mass. The solid red curve represents the TR noise of the ITM taking standing waves into account as the dashed black curve represents the result for a homogeneous readout neglecting standing waves. The diagram is scaled logarithmically on both axes with a factor of 10 between neighbored dashed lines. For silicon at 10 K region III is situated at frequencies above 10^9 Hz. The heat equation loses validity at these high frequencies. Thus, regions III and IV show no physical relevance for silicon. In contrast, for fused silica at room temperature region III shows physical relevance again as it starts at a frequency around 1 kHz [14].

the substrate. There the adiabatic boundary condition constrains the heat flow and, simply spoken, limits the amount of heat flowing from the center to the outer radial regions. Thus we have a nearly isothermal behavior leading to a constant TR noise contribution. Compared to the model of an infinite disc [11] the amount of dissipated energy and the TR noise level is decreased in the low frequency region. For our exemplary calculation at 1 Hz the model of the infinite disc provides a TR noise twice as high as our model of a finite-sized cylinder.

For higher frequencies the thermal path length will become short compared to the radial dimension of the test mass ($r_{\text{th}} < R$). Thus, no remarkable amount of heat is transported from the virtual heat source in the center of the cylinder to its circular boundaries. Therefore,

the approximation of a disc with infinite radius holds and our calculation should coincide with the results from Ref. [11]. This consideration is clearly confirmed by region II of Fig. 2. At frequencies above 100 Hz it shows a decrease of $\sqrt{S_z(\omega)} \propto 1/\omega$ validating our result.

The standing wave model introduces a modulation of the inserted heat along the z -direction with a characteristic length of $r_{\text{SW}} = 4\pi N/\lambda_0$. Now the same process discussed above occurs with the new geometric parameter $r_{\text{th}} \rightarrow r_{\text{SW}}$. Consequently, at a frequency around 10^9 Hz the dissipation is dominated by the heat flow along the z -direction. Again the noise spectrum remains at a constant level (region III) up to a frequency of 10^{14} Hz. At that point $r_{\text{th}} \approx r_{\text{SW}}$ and for higher frequencies another $1/f$ -decay of the TR noise amplitude is predicted (region IV).

Approaching phonon frequencies the transport theoretical derivation of the heat equation is likely to change. Thus, for our discussion of a silicon test mass at 10 K region III and IV do not play a physical role. But for fused silica the model of standing waves shows an impact at frequencies above 1 kHz [14] and should be taken into account.

Using the trigonometrical identity

$$\sin^2\left(\frac{2\pi N}{\lambda_0}z\right) = \frac{1}{2}\left(1 - \cos\left(2\frac{2\pi N}{\lambda_0}z\right)\right), \quad (35)$$

we can achieve an analytical understanding of this behavior. For the sake of simplicity let us assume a value in the argument of the cosine that corresponds to a specific l_m coefficient. Then the z -decomposition becomes easy as only two terms L_m appear, i.e., one at $m = 0$ and one at

$$l_{\hat{m}} = \hat{m}\frac{\pi}{H} = 2\frac{2\pi N}{\lambda_0} \Rightarrow \hat{m} = \frac{4HN}{\lambda_0} \approx 4 \times 10^6, \quad (36)$$

where the numerical estimate is due to the ET parameters.

An examination of Eq. (31) allows an analytical understanding of the obtained noise spectrum. Beginning at low frequencies the constant term $(\kappa/C_p k_n^2)^2$ due to the contribution of $m = 0$ dominates the denominator and thus no frequency dependence is observable. With increasing frequency the ω^2 -term dominates the denominator for $m = 0$ leading to the observed noise reduction. At even higher frequencies the contribution with $m \neq 0$ leads to the second plateau. Finally, at $\omega \approx \kappa/C_p l_m^2$ this plateau enters a $1/\omega$ decay.

C. Finite element analysis (FEA)

We further performed a finite element calculation of the dissipated heat W_{diss} and compared the results to our analytical calculation scheme. For this purpose we used the FE package COMSOL [27]. An efficient computation is only possible for the simple model as the advanced model

would require an element size below the wavelength in the substrate and thus more than 10^6 elements. The FEA results for the ET design at 10 K are presented as circles in Fig. 3. We obtain a significant coincidence between the FE results and the results of our analytical model. With a deviation of well below 1% the FE calculation strongly verifies the results of our analytical approach.

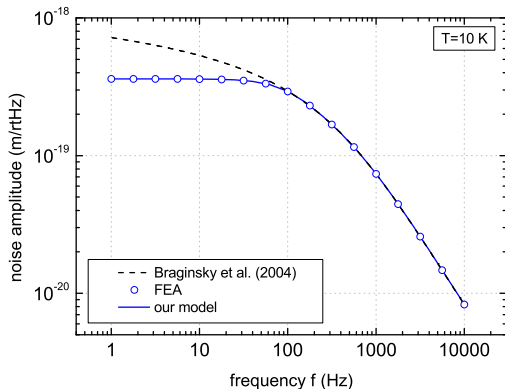


FIG. 3. The diagram shows the thermorefractive noise amplitude $\sqrt{S_z(f)}$ for a finite silicon cylinder of ET geometry (solid blue line) at 10 K compared to an FE calculation of the same geometry (blue circles). At frequencies above 100 Hz a coincidence with the model of an infinite disc [11] (dashed black line) is shown.

D. TR noise in a simplified interferometer

At this point we apply our results of TR noise to a simplified interferometer consisting of two arms with cavities and the beam splitter (BS) assuming the parameters of ET, LCGT, and CLIO. We begin with the calculation of the TR noise introduced by the ITM. As the ITM is present in both arms the resulting displacement noise power adds independently leading to a factor of two in front of the noise expression Eq. (31). In the cryogenic temperature range ($T_0 < 30$ K) and for interesting frequencies from 1 Hz to 10 kHz the contribution of standing waves to TR noise is negligible. The influence of the finite radial dimension can be realized at low temperatures and frequencies, where the growing thermal path length exceeds the radial dimension of the substrate. In sapphire the resulting constant noise level at low frequencies is extended to higher frequencies than in silicon. This behavior arises from the different thermal parameters which affect the thermal path length.

In addition we also calculated the TR noise introduced by the beam splitter $S_{BS}(\omega)$. As all interferometer designs feature beam splitters made of fused silica at room temperature, we used the theory described in Ref. [14] to

obtain the beam splitter noise levels

$$S_{BS}(\omega) = \frac{4k_B T_0^2 \kappa \beta^2}{\pi (C_p r_0^2 \omega)^2 \cos(i)} \frac{H}{2\eta^2} (\eta + \eta^{-1}) \times \left[1 + \frac{2k^2 r_0^2 \eta}{(\eta + \eta^{-1})(1 + (2kr_{th})^4)} \right]. \quad (37)$$

In this expression H is the height of the beam splitter, i is the incident angle of light within the beam splitter, and $H/\cos(i)$ is the length of the light's path through the beam splitter. η describes the ratio between the long and the short semiaxis of the elliptical beam within the beam splitter, $k = 2\pi N/\lambda_0$ is the wave vector of light within the substrate, and $r_{th} = \sqrt{\kappa/(\omega C_p)}$ is the thermal path length. The beam splitter introduces TR noise only to one arm of the interferometer.

We furthermore compare the obtained results to the standard quantum limit $S_{SQL}(\omega)$ of the simplified interferometer. Assuming identical ITMs and ETMs for a Michelson interferometer with arm cavities the expression for the SQL reads [28]

$$S_{SQL}(\omega) = \frac{8}{\omega^2} \frac{\hbar}{M}. \quad (38)$$

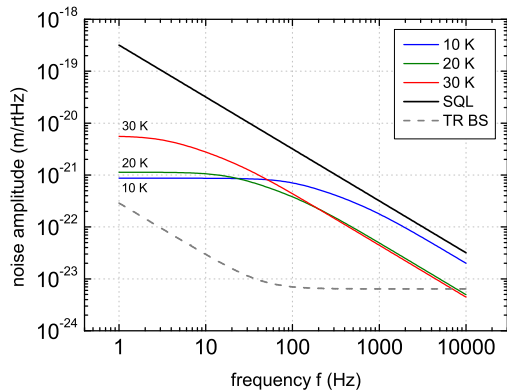
There M denotes the substrate mass, which is accessible by the information of Table II, and \hbar is the reduced Planck constant. Within this approach the beam splitter is considered to possess an infinite mass and, thus, not to affect the SQL.

A direct comparison of TR noise of the ITM or the BS with the standard quantum limit is only possible, if we account for the different positions within the interferometer. While TR noise in the BS and the ITM is situated outside the arm cavity, the SQL predicts the motion of the reflecting planes sensed by the light within the cavity. Consequently, this fact is considered by the introduction of a weighting factor $2F/\pi$ that weakens the effect of noise occurring outside the cavity. A detailed investigation of this weighting factor is given in App. E.

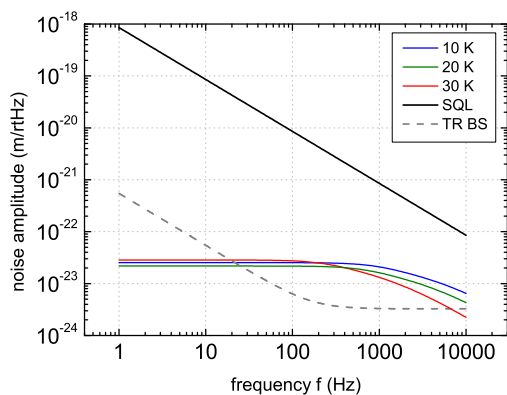
Finally, Fig. 4 illustrates the noise of the simple interferometer's output $S_{IF}(\omega)$ which is sensible to a differential optical path change in the arms. This noise variable is to be interpreted as a differential mirror motion of the arms. The ratio of this motion to the cavity length L corresponds to the amplitude of a gravitational wave. In Fig. 4 we compare the weighted TR displacement noise amplitude of the ITM $\pi/(2F) \times \sqrt{2S_z(\omega)}$ and the beam splitter $\pi/(2F) \times \sqrt{S_{BS}(\omega)}$ to the SQL of the simplified interferometer $\sqrt{S_{SQL}(\omega)}$.

V. DISCUSSION

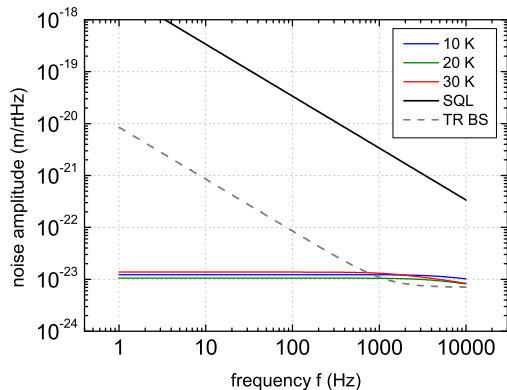
Applying our theory of TR noise for finite-sized test masses on cryogenic gravitational wave detectors as ET, LCGT, and CLIO reveals that the ITM TR noise is below the standard quantum limit for all detectors. For LCGT



(a)ET



(b)LCGT



(c)CLIO

FIG. 4. Numerical results for the thermorefractive noise amplitude at the output of a simplified interferometer $\sqrt{S_{IF}(f)}$. Solid lines represent our results considering the finite radial dimension of the ITM [Eq. (31)] for ET, LCGT, and CLIO at 10 K, 20 K, and 30 K. The dashed line indicates the TR noise of the fused silica beam splitter at 290 K. Also the standard quantum limit (SQL) of the simplified interferometers using the corresponding ITM geometry is shown.

and CLIO the TR noise of the ITM is more than one order below the SQL and, thus, negligible due to the low thermo-optic coefficient of sapphire and the small height of the ITM. The situation for the silicon test mass of ET-LF is different. At a temperature of 10 K and frequencies above 500 Hz the TR noise contribution of the ITM is only a factor of two below the SQL. Consequently, this noise source becomes important when the SQL is beaten, e.g., by utilizing squeezing in the detector [29]. At low frequencies the finite radial dimension of the test mass leads to a constant noise level far below the SQL. Compared to the theory of the infinite disc our finite model predicts a lower noise. A factor of 2 between both models is revealed for a silicon test mass at 10 K.

A crucial point in the noise estimate consists in the knowledge of the thermorefractive parameter β . For sapphire only an upper limit of 9×10^{-8} for temperatures below 40 K is known [26]. For silicon at 1550 nm only values down to 30 K are experimentally known [25] forcing us to use extrapolated values at low temperatures. Thus, a reliable estimate of TR noise in detector components demands precise experiments on the determination of β at low temperatures.

In optical micro resonators [4, 5, 8] we find systems with transmitted media within the cavity. There the effect of TR noise is amplified mainly by the finesse of the cavity. Thus, our results can have a possible influence on the resonator design in this field.

Next to thermorefractive noise also thermoelastic noise originates from thermal temperature fluctuations in the test mass. This common origin allows a collective treatment known as thermo-optic noise. It shows a suppression compared to the independent sum of the single contributions. Evans et al. [30] and Gorodetsky [31] showed that this treatment brings the single contributions far below the detectors sensitivity. Also the impact of finite-sized substrates on coating thermo-optic noise was investigated in 2009 [32]. A possible extension of our work involves the determination of the substrate thermo-optic noise for finite substrate geometries. This task remains open for future work.

VI. CONCLUSION

Investigating thermorefractive noise for crystalline materials at low temperatures desires the consideration of the finite dimensions of the sample. Next to this point also the interferometric effect of standing waves should be considered in a noise analysis. Our results containing both requirements were independently derived by Levin's and Langevin's approach. They were confirmed by a comparison to an FE analysis and to known special cases in the literature. Applying this model to cryogenic gravitational wave detectors reveals that thermorefractive noise in ET could become a problem at frequencies above 500 Hz while it can be neglected for LCGT and CLIO.

ACKNOWLEDGEMENT

We thank M. Ohashi, S. Miyoki, T. Uchiyama, and S. Telada for providing us with information about the specifications of the CLIO interferometer. We also thank Y. Levin for his helpful advices on the manuscript. D. Heinert and R. Nawrodt acknowledge the support of the German Science Foundation (DFG) under contract SFB Transregio 7. A. G. Gurkovsky and S. P. Vyatchanin have been supported by LIGO team from Caltech and in part by NSF and Caltech grant PHY-0967049 and grant 08-02-00580 from Russian Foundation for Basic Research.

Appendix A: Radiative heat transport

In the presented analysis the solution of the heat equation was derived assuming adiabatic boundary conditions. Using this approximation any heat transport via radiation is neglected. But as we are interested in the finite-size effects appearing at low frequencies the validity of the adiabatic assumption has to be proven. In this appendix we estimate the dissipated energy with respect to radiation.

In a first step we compare the amount of heat transported by radiation and conduction as given, e.g., in Ref. [33]. The amount of radiated heat can be calculated using the Stefan-Boltzmann law. In a rough approximation we identify the environmental temperature with the average temperature of the substrate T_0 . The radiated heat flow h normal to the surface then follows the relation

$$h_{\text{rad}} = \sigma(T^4 - T_0^4) \approx 4\sigma T_0^3 \delta T, \quad (\text{A1})$$

where σ is the Stefan-Boltzmann constant and T is the temperature of the substrate's surface. Introducing the temperature deviation $\delta T(t) = T(t) - T_0$ and expanding the Stefan-Boltzmann law to the leading order in δT revealed the approximation in the last step of Eq. (A1). This linear behavior is important as Levin's approach is only valid for linear systems. We compare this to the amount of heat transported to the boundary via conduction

$$h_{\text{cond}} = -\kappa \frac{\partial}{\partial r} T \simeq -\kappa \frac{\delta T}{r_{\text{th}}}. \quad (\text{A2})$$

Here the thermal path length $r_{\text{th}} = \sqrt{\kappa/(\omega C_p)}$ is used to estimate a typical value of $\partial T/\partial r$. Inserting the numerical values from the text into these equations confirms that the amount of heat radiation is negligibly small compared to heat conduction ($h_{\text{rad}} \lesssim 10^{-6} h_{\text{cond}}$). Consequently, the heat, which is virtually inserted at the center of the substrate and transported to the boundary by conduction, cannot be emitted due to radiation. This behavior justifies to neglect the effect of radiation in the solution of the heat equation.

Even if the radiated heat does not change the temperature distribution effectively, it produces an increase of

entropy leading to energy dissipation and thermal noise. At this point we want to give a second and more quantitative estimate of this effect. The first condition to allow for an effective radiation of heat consists in an effective heat conduction from the center to the boundary of the substrate. Thus, due to the periodically inserted heat we assume an instant temperature equalization within the substrate. This leads to a spatially constant temperature within the sample. Mathematically, the Laplace term in the heat equation [Eq. (7)] vanishes leading to

$$C_p (T(t) - T_0) = q(\vec{r}, t). \quad (\text{A3})$$

Using the definition of $q(\vec{r}, t)$ an integration over the substrate volume V reveals

$$\delta T(t) = \frac{1}{C_p V} \int_V q(\vec{r}, t) dr = \frac{\beta T_0 F_0}{C_p V} e^{i\omega t} = \delta \hat{T} e^{i\omega t}. \quad (\text{A4})$$

Here the term $\delta \hat{T}$ is introduced as the amplitude of temperature fluctuations. With the knowledge of the substrate temperature at the boundaries the amount of radiated heat can be calculated using Eq. (A1). As shown in the previous paragraph we can further assume that the heat transported via radiation is sufficiently small not to change the temperature distribution within the substrate.

Following Ref. [19] the increase of entropy is given as

$$\dot{S} = - \int_V \text{div} \left(\frac{\vec{h}}{T} \right) dV, \quad (\text{A5})$$

where \vec{h} represents the heat flow. Transforming this into a surface integral, replacing h by Eq. (A1), and expanding the denominator to small temperature changes results in

$$\dot{S}(t) = -4\sigma T_0^2 A \delta T(t) \left(1 - \frac{\delta T(t)}{T_0} \right), \quad (\text{A6})$$

where A represents the surface area undergoing radiation. In our estimate we consider the whole geometrical surface of the substrate as A . Only the term quadratic in δT enters the temporal average of the entropy increase. A multiplication with the average temperature then reveals the mean rate of energy dissipation due to radiation as

$$W_{\text{diss}} = T_0 f \int_0^{1/f} \dot{S}(t) dt = 2\sigma T_0^2 A \left| \delta \hat{T} \right|^2, \quad (\text{A7})$$

$$= 2\sigma T_0^4 \frac{A}{V^2} \frac{\beta^2}{C_p^2} F_0^2. \quad (\text{A8})$$

We have performed a numerical evaluation of the above equation for ET and LCGT at a frequency of 1 Hz. The result shows that the dissipation due to radiation will be 5 or 4 orders of magnitudes lower than the dissipation due to conduction for ET and LCGT, respectively. The change of the noise amplitude due to radiation would be

below 1% and, thus, can be omitted in our calculations heading for frequencies above 1 Hz. The estimate presented here predicts equal contributions of conduction and radiation at a frequency around 10^{-2} Hz.

Appendix B: Langevin approach

In this appendix we present details of the TR noise calculation using the Langevin approach for the simple and the advanced model.

1. Simple model

On our way to derive the noise spectrum we continue by calculating the autocorrelation function of the averaged temperature $\overline{T}(t)$. For this purpose we repeatedly use means of the Fourier transform of $T(\vec{r}, t)$ and insert it into Eq. (24). Due to the volume integration the dependence from the azimuthal and the z -coordinate vanishes. That allows us to focus our consideration on the radial variable. The Fourier coefficients of temperature and fluctuational force are connected by the heat equation. Using Eq. (22) a short calculation reveals the correlation of the remaining Fourier components $F_n(\omega)$

$$F(\vec{r}, t) = \int_{-\infty}^{\infty} \frac{d\omega}{2\pi} e^{i\omega t} \sum_{n=0}^{\infty} F_n(\omega) J_0(k_n r), \quad (\text{B1})$$

to be

$$\langle F_n(\omega) F_{n'}(\omega') \rangle = \frac{4k_B T_0^2}{H R^2} \times \frac{\kappa}{C_p^2} \frac{k_n^2}{[J_0(k_n R)]^2} \delta_{nn'} \delta(\omega - \omega'). \quad (\text{B2})$$

Please note, that the finite dimensions of the substrate are implicitly given in the choice of the basis function of the Fourier transform in Eq. (B1). Finally, we can calculate the autocorrelation function of the averaged temperature as

$$\langle \overline{T}(t) \overline{T}(t + \tau) \rangle = \frac{8}{\pi} k_B T_0^2 \frac{1}{H r_0^4} \frac{\kappa}{C_p^2} \times \int_{-\infty}^{\infty} \frac{d\omega}{2\pi} \sum_{n=1}^{\infty} \frac{k_n^2 R^2 e^{i\omega \tau}}{\omega^2 + \frac{\kappa^2}{C_p^2} k_n^4} \frac{K_n^2}{[J_0(k_n R)]^2}. \quad (\text{B3})$$

If we apply the Wiener-Khinchin-theorem [34] on the last expression the one-sided spectral noise density of the averaged temperature \overline{T} is determined as

$$S_{\overline{T}}(\omega) = \frac{16}{\pi} k_B T_0^2 \frac{1}{H r_0^4} \frac{\kappa}{C_p^2} \times \sum_{n=1}^{\infty} \frac{k_n^2 R^2}{\omega^2 + \frac{\kappa^2}{C_p^2} k_n^4} \frac{K_n^2}{[J_0(k_n R)]^2}. \quad (\text{B4})$$

With the relation

$$S_z(\omega) = \beta^2 H^2 S_{\overline{T}}(\omega), \quad (\text{B5})$$

the result coincides with Eq. (19).

2. Advanced model

To take the standing wave effect into account, we have to consider the z -dependence of the averaged temperature in the Langevin approach. Therefore, we have to expand the correlation factor of the Fourier components to an additional index m , describing the z -dependence

$$\langle F_{nm}(\omega) F_{n'm'}(\omega') \rangle = \frac{4k_B T_0^2}{H R^2} \frac{\kappa}{C_p^2} (2 - \delta_{0m}) \times \frac{k_n^2 + l_m^2}{[J_0(k_n R)]^2} \delta_{nn'} \delta_{mm'} \delta(\omega - \omega'). \quad (\text{B6})$$

By inserting the Fourier transform of $T(\vec{r}, t)$ into Eq. (34) the averaged temperature \overline{T} can be rewritten as a sum

$$\overline{T}(t) = \frac{2\pi R^2}{\pi r_0^2} \int_{-\infty}^{\infty} \frac{d\omega}{2\pi} e^{i\omega t} \sum_{n,m=0}^{\infty} T_{nm}(\omega) K_n L_m. \quad (\text{B7})$$

Taking into account the relation

$$T_{nm}(\omega) = \frac{F_{nm}(\omega)}{i\omega - (\kappa/C_p)(k_n^2 + l_m^2)}, \quad (\text{B8})$$

and the correlators (B6) one can calculate the correlation function of \overline{T}

$$B(\tau) \equiv \langle \overline{T}(t) \overline{T}(t - \tau) \rangle \quad (\text{B9}) \\ = \int_{-\infty}^{\infty} \frac{d\omega}{2\pi} e^{i\omega \tau} \frac{8}{\pi} k_B T_0^2 \frac{\kappa}{C_p^2} \frac{R^2}{H r_0^4} \times \sum_{n=0}^{\infty} \sum_{m=0}^{\infty} \frac{2}{(1 + \delta_{m0})^2} \frac{1}{[J_0(a_n)]^2} \times \frac{(1 + \delta_{m0}) k_n^2 + (1 - \delta_{m0}) l_m^2}{\omega^2 + \frac{\kappa^2}{C_p^2} (k_n^2 + l_m^2)} K_n^2 L_m^2.$$

Now applying the Wiener-Khinchin-theorem on the last expression one can find the one-sided spectral noise density $S_{\overline{T}}(\omega)$ of the averaged temperature and recalculate it into $S_z(\omega) = \beta^2 H^2 S_{\overline{T}}(\omega)$. The result coincides with Eq. (31) originating from Levin's approach.

Appendix C: Semi-qualitative considerations on the Langevin model

In this appendix we derive the dependence of the TR noise formula due to purely qualitative considerations.

TR noise can be described as an effective mirror motion Δz , which is given by

$$\Delta z = \beta H \sqrt{\langle \Delta T^2 \rangle_{V,\tau}}. \quad (\text{C1})$$

Please note that in contrast to the rest of the article the symbol Δ denotes variations instead of the Laplace operator throughout this appendix. Consequently, ΔT characterizes the temperature fluctuation within the substrate and the brackets denote a spatial averaging over the laser beam volume $V \simeq r_0^2 H$ as well as a temporal averaging over a time τ .

Assuming a characteristic time τ^* for thermal relaxation processes allows us to give an approximation for the averaged temperature fluctuations

$$\langle \Delta T^2 \rangle_{V,\tau} \simeq \frac{k_B T_0^2}{C_p V} \times \begin{cases} \frac{\tau}{\tau^*}, & \text{if } \tau \ll \tau^* \\ 1, & \text{if } \tau \simeq \tau^* \\ \frac{\tau^*}{\tau}, & \text{if } \tau \gg \tau^* \end{cases}. \quad (\text{C2})$$

At short observation times $\tau < \tau^*$ the thermal mass prevents an effective propagation of heat through the borders of the sample volume, that is probed by the laser beam and, thus, leads to a vanishing temperature change for $\tau \rightarrow 0$. At long observation times $\tau > \tau^*$ the perturbations are quickly balanced and averaged to zero for $\tau \rightarrow \infty$. In between both limits heat is effectively flowing out of the probed volume while the time τ is short enough to avoid an averaging to zero. According to this behavior we find a maximum of temperature fluctuations at $\tau \simeq \tau^*$.

We denote the minimum size of the probed volume V as a . Note that the thermal relaxation time is connected to this size a via $\tau^* \simeq a^2 C_p / \kappa$. Now we apply our considerations to the different noise regimes, illustrated in Fig. 2. Beginning at long observation times at first the laser beam radius is the significant length ($a \simeq r_0, \tau_r^*$) while at shorter observation times the standing wave pattern along the laser beam becomes important ($a \simeq \lambda, \tau_\lambda^*$).

Range I ($\tau \gg \tau_r^* \gg \tau_\lambda^*$) From Eqs. (C1) and (C2) we find an effective mirror displacement of

$$\Delta z \simeq \beta H \sqrt{\frac{k_B T_0^2}{C_p r_0^2 H}} \sqrt{\frac{\tau^*}{\tau}}. \quad (\text{C3})$$

Taking into account the definition of the power noise spectrum $S_z(\omega)$

$$\Delta z^2 \simeq S_z(\omega) \Delta \omega, \quad (\text{C4})$$

and using $\Delta \omega \simeq \omega \simeq 1/\tau$ yields

$$S_I(\omega) \simeq \frac{\Delta z^2}{\omega} \simeq \beta^2 H \frac{k_B T_0^2}{\kappa}. \quad (\text{C5})$$

The same result is obtained by utilizing a second approach employing the thermal path length $r_{\text{th}} = \sqrt{\kappa/(\omega C_p)}$. There we consider volumes of $\simeq r_{\text{th}}^3$ to show independent temperatures. The total number of independent regions in the probed volume is about $\simeq H/r_{\text{th}}$. The averaged temperature fluctuation is proportional to the reciprocal of this number and reads

$$\langle \Delta T^2 \rangle \simeq \frac{r_{\text{th}}}{H} \times \frac{k_B T_0^2}{C_p r_{\text{th}}^3}. \quad (\text{C6})$$

This result leads to the same noise spectrum as given before in Eq. (C5).

Range II ($\tau_r^* \gg \tau \gg \tau_\lambda^*$) By using the corresponding term in Eq. (C2) and following the same scheme as above we obtain

$$S_{\text{II}}(\omega) \simeq \beta^2 H \frac{k_B T_0^2 \kappa}{C_p^2 r_0^4 \omega^2}. \quad (\text{C7})$$

Range III ($\tau_r^* \gg \tau \gg \tau_\lambda^*$) In this frequency range the fluctuations due to the standing waves dominate the spectrum. To take standing waves into account we only have to replace τ_r^* by τ_λ^* in the results of Range I and II. This leads to

$$S_{\text{III}}(\omega) \simeq \beta^2 H \frac{k_B T_0^2 \lambda^2}{\kappa r_0^2}. \quad (\text{C8})$$

Range IV ($\tau_r^* \gg \tau_\lambda^* \gg \tau$) At very short observation times we find

$$S_{\text{IV}}(\omega) \simeq \beta^2 H \frac{k_B T_0^2 \kappa}{C_p^2 r_0^2 \lambda^2 \omega^2}. \quad (\text{C9})$$

Compared to the analytical results all our semi-qualitative time domain considerations provide the correct dependence on physical parameters.

Appendix D: Standing wave term

To obtain Levin's \sin^2 -term in the inserted entropy one has to consider the phase change of the reflected light due to a temperature variation within the substrate. These temperature variations lead to a variation of the refractive index $dN = \beta dT$. For simplicity we start with the case where only a small area is affected by an index change dN .

1. Model

For the calculation of the phase change we apply the analogy of optical layer stacks to electrical transmission lines [35]. This analogy is easily illustrated for the special case of normal incidence. There we assume the incoming electromagnetic wave to travel along the z -direction and the electric field E to be polarized along the y -direction. For homogeneous and isotropic optical layers, then the magnetic field H reveals to be polarized along the x -direction. Perpendicular to the z -direction the layer geometry is homogeneous. Thus, we postulate only a z -dependence for E and H . Applying Maxwell's equations

$$\nabla \times \vec{E} = -\mu_0 \mu_r \partial_t \vec{H}, \quad (\text{D1})$$

$$\nabla \times \vec{H} = -\epsilon_0 \epsilon_r \partial_t \vec{E}, \quad (\text{D2})$$

and utilizing the Fourier transform into the frequency domain yields a description of the electromagnetic fields

within a single layer

$$\partial_z E_y(z) = \mu_0 \mu_r i \omega H_x(z) , \quad (\text{D3})$$

$$\partial_z H_x(z) = \epsilon_0 \epsilon_r i \omega E_y(z) . \quad (\text{D4})$$

Here μ_0 and μ_r are the vacuum and the relative permeability, respectively, and ϵ_0 and ϵ_r are the vacuum and the relative permittivity, respectively. The differential equations describing an electric transmission line show the same structure. We find them by replacing E_y as voltage and H_x as current. The final step in the analogy compares the boundary conditions of both problems. Maxwell's equations predict a continuous transition for E_y and H_x as they are perpendicular to the normal of the boundary between two layers. In the transmission line model voltage and current also show a continuous behavior at the boundaries completing our analogy.

Following these steps we find a wave resistance of

$$\rho = \sqrt{\frac{\mu_0 \mu_r}{\epsilon_0 \epsilon_r}} . \quad (\text{D5})$$

We are only interested in the ratio between two impedances and, thus, can omit the constant factors μ_0 and ϵ_0 . Furthermore we approximate our layer materials as non-magnetic, i.e., $\mu_r = 1$. Using the relation $N^2 = \epsilon_r$ one has to identify the wave resistance with the inverse refractive index ($\rho = 1/N$) in the transmission line model. Then the coefficients of amplitude reflectivity are connected to impedances of the subsystems Z_i .

Fig. 5 illustrates the transmission line analogue of the ITM. In this sketch light is approaching from the left and is reflected to the left again. In our calculation we neglect the left boundary of the ITM as it shows an anti-reflective coating in the detector. At $z = 0$ we assume the disturbed region with a slightly differing resistance $\rho + \delta\rho$ with $\delta\rho \ll \rho$. Its length ℓ should be small in a way to satisfy $k_0 \ell / \rho \ll 1$. Here $k_0 = 2\pi/\lambda_0$ represents the vacuum light wave vector.

The disturbance should be the length L apart from the right boundary of the ITM. Thus from $z = \ell$ to $z = L + \ell$ we assume an undisturbed substrate. Finally at $z = L + \ell$ there occurs an approximately perfect reflection due to the resonant arm cavity, which is accounted for by a short-circuited end in the transmission line model.

2. Calculations

The analysis is performed from the short-circuited end to the left, i.e., in decreasing z -direction. We further introduce the following variables

$$\phi = \frac{k_0 \ell}{\rho} , \quad \psi = \frac{k_0 L}{\rho} , \quad (\text{D6})$$

$$\vartheta = e^{i\phi} , \quad \theta = e^{i\psi} , \quad (\text{D7})$$

$$\bar{\vartheta} = e^{ik_0 \ell / (\rho + \delta\rho)} \simeq \vartheta \left(1 - i\phi \frac{\delta\rho}{\rho} \right) . \quad (\text{D8})$$

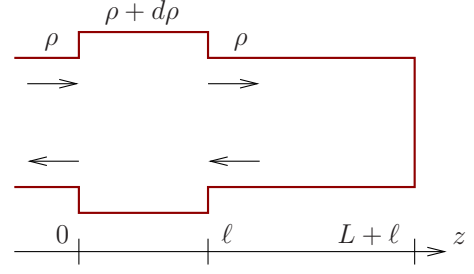


FIG. 5. Sketch of the ITM geometry underlying the derivation of the \sin^2 -term due to standing waves. A small temperature fluctuation at a distance L apart from the end of the ITM is assumed.

At the short-circuited end ($z = L + \ell$) the impedance $Z_{L+\ell}$ and the amplitude reflectivity $R_{L+\ell}$ are

$$Z_{L+\ell} = 0 , \quad (\text{D9})$$

$$R_{L+\ell} = \frac{Z_{L+\ell} - \rho}{\rho + Z_{L+\ell}} = -1 . \quad (\text{D10})$$

At the boundary to the disturbed substrate region ($z = \ell$) the impedance and the reflectivity are

$$Z_\ell = \rho \frac{1 + R_{L+\ell} \theta^2}{1 - R_{L+\ell} \theta^2} = \rho \frac{1 - \theta^2}{1 + \theta^2} , \quad (\text{D11})$$

$$\begin{aligned} R_\ell &= \frac{Z_\ell - \rho - \delta\rho}{\rho + \delta\rho + Z_\ell} = -\frac{2\rho\theta^2 + \delta\rho(1 + \theta^2)}{2\rho + \delta\rho(1 + \theta^2)} \\ &\simeq -\theta^2 \left(1 + \frac{\delta\rho}{2\rho} \left[\frac{1}{\theta^2} - \theta^2 \right] \right) . \end{aligned} \quad (\text{D12})$$

In the last equation we used the approximation of small fluctuations $\delta\rho \ll \rho$.

Finally, at our coordinate origin ($z = 0$) we obtain the reflectivity R_0 as the main point of our interest

$$R_0 = \frac{Z_0 - \rho}{\rho + Z_0} , \quad Z_0 = (\rho + \delta\rho) \frac{1 + R_\ell \bar{\vartheta}^2}{1 - R_\ell \bar{\vartheta}^2} . \quad (\text{D13})$$

Now we expand the expression for R_0 into a series keeping only terms proportional to $\delta\rho$, ϕ , and the cross term $\phi \delta\rho$. We end up with the following expression

$$\begin{aligned} R_0 &\simeq -\theta^2 (1 + 2i\phi) - i\phi \frac{\delta\rho}{\rho} [1 - \theta^2]^2 \\ &= -\theta^2 \left(1 + 2i\phi + i\phi \frac{\delta\rho}{\rho} \left[\frac{1}{\theta} - \theta \right]^2 \right) \\ &= -\theta^2 \left(1 + \frac{2ik_0 \ell}{\rho} - \frac{4ik_0 \ell \delta\rho}{\rho^2} \sin^2 \frac{k_0 L}{\rho} \right) . \end{aligned} \quad (\text{D14})$$

Here the last term in brackets including $\delta\rho$ is responsible for TR noise. There we find the characteristic \sin^2 -dependence emerging from standing waves in the substrate.

From the relation $N = 1/\rho$ it follows that $\delta N = -\delta\rho/\rho^2$ and, thus,

$$R_0 \simeq -\theta^2 (1 + 2ik_0 \ell N + ik_0 \ell \delta N 4 \sin^2(kL)) . \quad (\text{D15})$$

Note the difference between the wave vector in vacuum k_0 and in the substrate $k = k_0 N$ in the above expression.

3. Thermorefractive noise phase shift

From the previous subsection we know the phase change due to a temperature change in a thin layer of thickness ℓ . The phase change of the reflected beam $\Delta\phi$ then reads

$$\Delta\phi = 4k_0 \delta N \ell \sin^2(kL) . \quad (\text{D16})$$

In our linear analysis this behavior can be generalized to the case of steady refractive index characteristics $N(z) = N + \delta N(z)$. Then the length of the disturbed piece becomes a differential $\ell \rightarrow dz$. For a substrate with height H we find

$$\Delta\phi \simeq \int_0^H 4k_0 \delta N(z) \sin^2(kL) dz , \quad (\text{D17})$$

where the length L becomes dependent from the z -coordinate ($L \rightarrow H - z$). This introduces an additional angular component $\varphi_0 = kH$ into our final equation

$$\Delta\phi \simeq \int_0^H 4k_0 \delta N(z) \sin^2(kz - \varphi_0) dz . \quad (\text{D18})$$

As our problem – and especially the fluctuation of the refractive index δN – exhibits a mirror symmetry with respect to the plane at $z = H/2$ we can perform a variable transformation $z \rightarrow H - z$ without affecting the results. Then we obtain Eq. (D18) with $\varphi_0 = 0$, i.e., we can neglect the effect of a phase shift. If the arm cavity is brought out of resonance, the phase shift φ_0 will have to be considered again.

Appendix E: Weighting factor for noise sources inside and outside the arm cavity

To compare our obtained noise level with the noise spectrum of an end mirror, we have to consider that optical components within the arm cavity are probed more often than the components outside the cavity. Thus the weighting factor should depend on the finesse as a measure of effective roundtrips of light within the cavity. A rigorous calculation bases on the investigation of the phase of the reflected light.

In this section we calculate the total noise for one optical device outside the cavity (e.g., TR noise of ITM) together with the cavity mirrors (the known noise processes for an end mirror are transformed to effective mirror motions). The problem geometry is presented in Fig. 6. Thereby the electric field amplitudes of the incoming and reflected light E_{in} and E_{out} satisfy the equation

$$\frac{E_{\text{out}}}{E_{\text{in}}} = e^{2i\varphi} e^{i2kx_1} \frac{r_1 + r_2 e^{2i\theta}}{1 + r_1 r_2 e^{2i\theta}} . \quad (\text{E1})$$

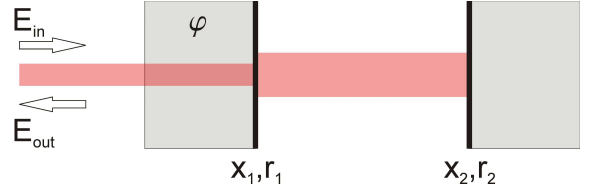


FIG. 6. Schematic view of an interferometer arm with noise variables inside the arm cavity (mirror positions x_1, x_2) and outside the cavity (φ , e.g., TR noise of ITM).

Here $\theta = k(L + x_2 - x_1)$ represents the phase change due to a single pass of the cavity while r_1 and r_2 represent the amplitude reflectivities of the mirrors. The phase advance φ can be interpreted as an equal position change kx_{out} . Expanding this expression to linear terms around the resonant state [$\exp(2ikL) = -1$] results in

$$\frac{E_{\text{out}}}{E_{\text{in}}} = A_0 + 2ik [A_{\text{out}} \Delta x_{\text{out}} + A_1 \Delta x_1 + A_2 \Delta x_2] , \quad (\text{E2})$$

with

$$A_0 = \frac{r_1 - r_2}{1 - r_1 r_2} , \quad (\text{E3})$$

$$A_{\text{out}} = \frac{r_1 - r_2}{1 - r_1 r_2} , \quad (\text{E4})$$

$$A_1 = r_1 \frac{1 - 2r_1 r_2 + r_2^2}{(1 - r_1 r_2)^2} , \quad (\text{E5})$$

$$A_2 = r_2 \frac{-1 + r_1^2}{(1 - r_1 r_2)^2} . \quad (\text{E6})$$

From the coefficients A_i one can easily calculate the weighting factor and perform a direct comparison between thermal noise sources inside (x_1, x_2) and outside the cavity (x_{out}). Thermal noise S_{out} introduced via the position x_{out} can be transformed to an equivalent inner cavity noise spectrum as

$$S_{x_1} = \left| \frac{A_{\text{out}}}{A_1} \right|^2 S_{\text{out}} , \quad (\text{E7})$$

$$S_{x_2} = \left| \frac{A_{\text{out}}}{A_2} \right|^2 S_{\text{out}} . \quad (\text{E8})$$

The coefficients above reveal to be

$$\left| \frac{A_1}{A_{\text{out}}} \right| = \left| \frac{r_1}{r_2 - r_1} + \frac{1}{1 - r_1 r_2} - 1 \right| , \quad (\text{E9})$$

$$\left| \frac{A_2}{A_{\text{out}}} \right| = \left| \frac{r_1}{r_2 - r_1} + \frac{1}{1 - r_1 r_2} \right| . \quad (\text{E10})$$

One can further simplify these expressions with the help of the cavity finesse F , which is defined as the ratio between the spectral distance of two neighboring transmission maxima and the width of such a maximum. The

finesse of a Fabry-Perot-cavity can be expressed as

$$F = \pi \frac{\sqrt{r_1 r_2}}{1 - r_1 r_2} . \quad (\text{E11})$$

Assuming a perfect end mirror $r_2 = 1$ and a high reflective input mirror $r_1 \approx 1$ one can show the equivalence of

$$\left| \frac{A_2}{A_{\text{out}}} \right| \approx \frac{2}{\pi} F . \quad (\text{E12})$$

For cavities with moderately high finesse ($F > 100$) we can further neglect the difference for the input and the end test mass and obtain a practical approximation for the weighting factor of

$$\left| \frac{A_1}{A_{\text{out}}} \right| \approx \left| \frac{A_2}{A_{\text{out}}} \right| \approx \frac{2}{\pi} F . \quad (\text{E13})$$

Appendix F: Approximations

In this section we specialize our results to regimes well known from former publications. At first we derive useful equations remembering the general steps of our analysis. Here we start with the introduced heat q concerning only the radial r -dependence

$$q(r) = Q \exp\left(-\frac{r^2}{r_0^2}\right) . \quad (\text{F1})$$

Then a Fourier transform was applied utilizing basis functions ($r = \rho R$)

$$f_n(\rho) = J_0(a_n \rho) , \quad (\text{F2})$$

and the scalar product of

$$\langle f(\rho), g(\rho) \rangle = \int_0^1 f(\rho) g^*(\rho) \rho d\rho , \quad (\text{F3})$$

where the star denotes the complex conjugate. From the choice of our basis functions f_n we obtain the normalization

$$\langle f_n, f_m \rangle = \frac{1}{2} [J_0(a_n)]^2 \delta_{nm} . \quad (\text{F4})$$

Consequently, the Fourier coefficients of $q(r)$ read

$$q_n = \frac{2}{[J_0(a_n)]^2} \underbrace{\langle q(r), f_n(r) \rangle}_{=QK_n} . \quad (\text{F5})$$

Now we apply Parseval's theorem on the function $q(r)$ obtaining

$$\begin{aligned} \langle q(\rho), q(\rho) \rangle &= \left\langle \sum_{n=0}^{\infty} q_n f_n(\rho), \sum_{m=0}^{\infty} q_m f_m(\rho) \right\rangle \\ &= \sum_{n=0}^{\infty} \frac{2}{[J_0(a_n)]^2} |QK_n|^2 . \end{aligned} \quad (\text{F6})$$

On the other hand the integration of $q(r)$ reveals

$$\begin{aligned} \langle q(\rho), q(\rho) \rangle &= \int_0^1 |Q|^2 \exp\left(-2\frac{\rho R}{r_0}\right) \rho d\rho \\ &= |Q|^2 \frac{r_0^2}{4R^2} \left[1 - \exp\left(-2\frac{R^2}{r_0^2}\right) \right] . \end{aligned} \quad (\text{F7})$$

As the second term in brackets is closely connected to clipping loss of a mirror and gravitational wave detectors are designed to show clipping losses far below 1% we can neglect this term in the further analysis. Using this approximation we arrive at a first important relation

$$\sum_{n=0}^{\infty} \frac{2|K_n|^2}{[J_0(a_n)]^2} \approx \frac{r_0^2}{4R^2} . \quad (\text{F8})$$

In a second step we repeat the same calculation with the spatial derivative of the introduced heat $q \rightarrow q' = \partial_r q(r)$. Using Eq. (17) we obtain

$$\sum_{n=0}^{\infty} \frac{4a_n^2 |K_n|^2}{[J_0(a_n)]^2} \approx 1 , \quad (\text{F9})$$

as the second relation necessary for our approximations.

We begin with the simplification of Eq. (19) neglecting the effect of standing waves as

$$\begin{aligned} S_z(\omega) &= \frac{4}{\pi} \frac{k_B T_0^2}{\omega^2} \frac{H}{r_0^4} \frac{\kappa \beta^2}{C_p^2} \\ &\times \sum_{n=0}^{\infty} \frac{4K_n^2}{[J_0(a_n)]^2} \frac{a_n^2}{1 + \frac{\kappa^2 a_n^4}{C_p^2 \omega^2 R^4}} . \end{aligned} \quad (\text{F10})$$

In the above expression we find the thermal path length in the denominator as

$$r_{\text{th}} = \sqrt{\kappa / (C_p \omega)} . \quad (\text{F11})$$

For the adiabatic case r_{th} approaches zero and no heat is transported within the substrate. As the analytical equivalent of this behavior we can simplify the denominator to the value of 1. Utilizing Eq. (F9) reveals

$$S_z(\omega) \approx \frac{4}{\pi} \frac{k_B T_0^2}{\omega^2} \frac{H}{r_0^4} \frac{\kappa \beta^2}{C_p^2} , \quad (\text{F12})$$

coinciding with the adiabatic result presented by Braginsky and Vyatchanin [11].

A useful second approximation can be applied to Eq. (31) where standing waves were considered. In a typical substrate we find about a million periods of the imaginary heat inside the substrate. Thus, the influence of the boundary on the heat flow along the z -direction is negligibly small and we can omit the boundary conditions along the z -direction. Then only two values for L_m remain (cf. argumentation in Sec. IV B), i.e., $L_0 = 1$ and $L_{\hat{m}} = 1/2$. For typical laser beam radii and substrate

radii only the first values for k_n show a remarkable impact on the result. These values are small compared to the coefficient l_m for the standing wave effects. Considering the relation $k_n \ll l_m$ we arrive at an approximate noise spectrum

$$S_z^{(\text{SW})}(\omega) \approx \frac{16}{\pi} k_B T_0^2 \frac{\kappa \beta^2}{C_p^2} \frac{H R^2}{r_0^4} \times \left(\sum_{n=0}^{\infty} \frac{1}{[J_0(a_n)]^2} \frac{k_n^2}{\omega^2 + \frac{\kappa^2}{C_p^2} k_n^4} K_n^2 + \sum_{n=0}^{\infty} \frac{2K_n^2}{[J_0(a_n)]^2} \frac{l_m^2}{\omega^2 + \frac{\kappa^2}{C_p^2} \frac{l_m^4}{4}} \frac{1}{4} \right). \quad (\text{F13})$$

The first sum in brackets reveals to be the result from

the simple case [cf. Eq. (19)]. Using Eq. (F8) and the relation $l_m = 2k$, where k is the wave vector within the substrate material we find

$$S_z^{(\text{SW})} \approx S_z^{(\text{hom})} + \frac{4}{\pi} \frac{k_B T_0^2}{\omega^2} \frac{\kappa \beta^2}{C_p^2} \frac{H}{r_0^2} \frac{k^2}{1 + (2kr_{\text{th}})^4}. \quad (\text{F14})$$

The effect of standing waves shows only an adding contribution to the result of the simple case. This additional contribution coincides with the result presented by Benthem and Levin [14] for normal incidence. It marks a useful approximation taking into account the substrate's finite radial dimension as well as standing waves within the substrate.

-
- [1] R. Nawrodt, S. Rowan, J. Hough, M. Punturo, F. Ricci, and J. Y. Vinet, *Gen. Relativ. Gravit.* **43**, 593 (2011).
- [2] K. Arai *et al.*, *Class. Quantum Grav.* **26**, 204020 (2009).
- [3] D. Sigg, *Class. Quantum Grav.* **25**, 114041 (2008).
- [4] A. B. Matsko, A. A. Savchenkov, N. Yu, and L. Maleki, *J. Opt. Soc. Am. B* **24**, 1324 (2007).
- [5] A. A. Savchenkov, A. B. Matsko, V. S. Ilchenko, N. Yu, and L. Maleki, *J. Opt. Soc. Am. B* **24**, 2988 (2007).
- [6] S. Knudsen, A. B. Tveten, and A. Dandridge, *IEEE Photon. Techn. Lett.* **7**, 90 (1995).
- [7] M. L. Gorodetsky and I. S. Grudin, *J. Opt. Soc. Am. B* **21**, 697 (2004).
- [8] G. Anetsberger, E. Gavartin, O. Arcizet, Q. P. Unterreithmeier, E. M. Weig, M. L. Gorodetsky, J. P. Kotthaus, and T. J. Kippenberg, *Phys. Rev. A* **82**, 061804(R) (2010).
- [9] K. Numata, A. Kemery, and J. Camp, *Phys. Rev. Lett.* **93**, 250602 (2004).
- [10] V. B. Braginsky, M. L. Gorodetsky, and S. P. Vyatchanin, *Phys. Lett. A* **271**, 303 (2000).
- [11] V. B. Braginsky and S. P. Vyatchanin, *Phys. Lett. A* **324**, 345 (2004).
- [12] Y. Levin, *Phys. Rev. D* **57**, 659 (1998).
- [13] Y. Levin, *Phys. Lett. A* **372**, 1941 (2008).
- [14] B. Benthem and Y. Levin, *Phys. Rev. D* **80**, 062004 (2009).
- [15] J. Franc, J. Degallaix, and R. Flaminio, (2010), ET note ET-0095C-10, available at www.et-gw.eu.
- [16] S. Hild, (2010), ET note ET-0136A-10, available at www.et-gw.eu.
- [17] H. B. Callen and T. A. Welton, *Phys. Rev.* **83**, 34 (1951).
- [18] M. Abramowitz and I. Stegun, eds., *Handbook of Mathematical Functions* (1964).
- [19] L. D. Landau and E. M. Lifshitz, *Theory of Elasticity* (Pargamon Press, New York, 1986).
- [20] P. Langevin, *C. R. Acad. Sci.* **146**, 530 (1908).
- [21] K. M. van Vliet, A. van der Ziel, and R. R. Schmidt, *J. Appl. Phys.* **51**, 2947 (1980).
- [22] S. Hild *et al.*, *Class. Quantum Grav.* **28**, 094013 (2011).
- [23] R. Hull, ed., *Physical properties of Crystalline Silicon* (INSPEC, The Institution of Electrical Engineers, London, 1999).
- [24] Y. S. Touloukian, *Thermophysical properties of matter* (IFI/Plenum, New York-Washington, 1970).
- [25] B. J. Frey, D. B. Leviton, and T. J. Madison, [arxiv:physics/0606168v1](https://arxiv.org/abs/physics/0606168v1).
- [26] T. Tomaru, T. Suzuki, S. Miyoki, T. Uchiyama, C. T. Taylor, A. Yamamoto, T. Shintomi, M. Ohashi, and K. Kuroda, *Class. Quantum Grav.* **19**, 2045 (2002).
- [27] www.comsol.com.
- [28] V. B. Braginsky and F. Y. Khalili, *Quantum Measurement*, edited by K. S. Thorne (Cambridge University Press, Cambridge, 1992).
- [29] C. M. Caves, *Phys. Rev. D* **23**, 1693 (1981).
- [30] M. Evans, S. Ballmer, M. Fejer, P. Fritschel, G. Harry, and G. Ogil, *Phys. Rev. D* **78**, 102003 (2008).
- [31] M. L. Gorodetsky, *Phys. Lett. A* **372**, 6813 (2008).
- [32] K. Somiya and K. Yamamoto, *Phys. Rev. D* **79**, 102004 (2009).
- [33] V. B. Braginsky, M. L. Gorodetsky, and S. P. Vyatchanin, *Phys. Lett. A* **264**, 1 (1999).
- [34] F. Reif, *Fundamentals of Statistical and Thermal Physics* (McGraw-Hill, 1965).
- [35] S. Solimeno, B. Crosignani, and P. Diporto, *Diffraction and Confinement of Optical Radiation* (Academic Press, 1986).